

ars548_ros: An ARS 548 RDI radar driver for ROS

F. Fernández-Calatayud L. Coto D. Alejo
J. J. Carpio F. Caballero L. Merino

June 21, 2024

Abstract

The ARS 548 RDI Radar is a premium model of the fifth generation of 77 GHz long range radar sensors with new RF antenna arrays, which offer digital beam forming. This radar measures independently the distance, speed and angle of objects without any reflectors in one measurement cycle based on Pulse Compression with New Frequency Modulation [1]. Unfortunately, to the best of our knowledge, there are no open source drivers available for Linux systems to enable users to analyze the data acquired by the sensor. In this paper, we present a driver that can interpret the data from the ARS 548 RDI sensor and make it available over the Robot Operating System versions 1 and 2 (ROS and ROS2). Thus, these data can be stored, represented, and analyzed using the powerful tools offered by ROS. Besides, our driver offers advanced object features provided by the sensor, such as relative estimated velocity and acceleration of each object, its orientation and angular velocity. We focus on the configuration of the sensor and the use of our driver including its filtering and representation tools. Besides, we offer a video tutorial to help in its configuration process. Finally, a dataset acquired with this sensor and an Ouster OS1-32 LiDAR sensor, to have baseline measurements, is available, so that the user can check the correctness of our driver [2].

keywords: ROS ; Linux driver ; Radar Sensor

Current code version	1.0.0
Permanent link to code/repository used for this code version	https://github.com/robotics-upo/ars548_ros
Permanent link to Reproducible Capsule	
Legal Code License	BSD 3-Clause License
Code versioning system used	Git
Software code languages, tools, and services used	C++, C.
Compilation requirements, operating environments & dependencies	Linux
If available Link to developer documentation/manual	https://github.com/robotics-upo/ars548_ros/blob/master/Readme.md
Support email for questions	dalejo@us.es

Code metadata

Software metadata

Current software version	1.0.0
Permanent link to executables of this version	
Permanent link to Reproducible Capsule	
Legal Software License	List one of the approved licenses
Computing platforms/Operating Systems	Linux
Installation requirements	ROS2 Humble or ROS Noetic
Support email for questions	dalejo@us.es

1 Motivation and significance

Autonomous navigation in reduced visibility scenarios, i.e. scenarios with the presence of fog, rain, dust or smoke, is still a great challenge for robots, as the prevalent sensors used for obstacle detection in robotics, i.e. Light Detection and Ranging sensors (LiDAR), RGB and RGB-D cameras, can significantly reduce their precision or become useless when operating under these conditions [3, 4]. Also, sensors onboard a smartphone can be used in robotic applications thanks to applications such as GetSensorData [5], but the performance of most onboard sensors would also drop in reduced

visibility scenarios. Therefore, different sensors should be employed to allow autonomous robots to be deployed in reduced visibility scenarios.

One alternative can be the use of thermal infrared cameras for odometry and localization [6, 7]. In this paper, we focus on RAdio Detection And Ranging sensors (radar), as aerosols do not affect them because their wavelength is larger than most aerosol particles. Thus, radar sensors are able to penetrate rain, dust and smoke. However, using a larger wavelength also has drawbacks, as the measurements obtained by a radar sensor have worse distance and angular accuracy and resolution when compared to LiDAR measurements [8].

Localization and navigation in reduced-visibility conditions is an active research field in autonomous car navigation. In fact, the vast majority of reduced-visibility datasets include radar information [9, 10, 11]. A common approach is to perform data fusion [12] of information perceived from LiDAR and radar sensors to ensure that the objects are detected in all circumstances. Unfortunately, the rotating radar sensors used in these datasets (such as the Navtech Radar CTS350-X) are too expensive and heavy to be included in a cost-effective robotic solution.

In the past years, advances in Frequency-Modulated Continuous Wave (FMCW) radar, which are based on the Doppler-effect to detect surrounding objects, have allowed the development of new radar sensors for robotic applications. Not only are these sensors able to detect the distance of nearby objects to them, but they can also estimate their relative velocity by taking advantage of Doppler effect. This velocity information can be used to improve the odometry estimation in harsh environments [13], which is fundamental for the safe autonomous navigation of robots. Still, their use for 3D navigation is challenging due to the low resolution and narrow vertical Field of View (FoV) of inexpensive models, such as the IWR6843 from Texas Instruments. More recently, the ARS 548 RDI sensor from Continental (see Figure 1) has been developed. It uses more advanced modulation techniques to better estimate the position and velocity of nearby objects. We believe that this sensor can be a good option for enabling a mobile robot or autonomous car to operate in reduced visibility scenarios, as it is a good compromise solution between inexpensive but feature lacking FMCW radar sensors and 2D rotating radars used for automotive purposes. Unfortunately, we did not find any open source driver that would allow us to acquire and process the data acquired from this sensor.

In this paper, we describe the architecture of the `ars548.ros` package. We



Figure 1: Continental ARS 548 RDI high resolution radar sensor.

highlight its interface to both versions of the Robotic Operating System [14] (ROS), which are becoming the standard for robotic development at least for academic purposes, even though ROS2 is more industrial focused than its predecessor, ROS. To develop ROS and ROS2 interfaces is very convenient as it allows us to use its representation, logging and processing tools. Hereinafter, we will use ROS when we refer to both versions of ROS. We illustrate the good performance of our driver by including data collected from real experiments with measurements of a OS1-32 LiDAR sensor from Ouster as a baseline. Finally, the driver is distributed in the BSD 3-Clause License in the hope that it will be helpful to the community.

2 Software description

We developed our driver with two main objectives in mind. On the one hand, our driver generates standard ROS messages such as `PointCloud2` that include information of the position and relative velocity, if available, of the detected points and objects; and `PoseArray` that indicates the direction of the movement of the detected objects. By using standard messages, the user can take advantage of existing representation and processing tools available in ROS. On the other hand, we are interested in providing the user with all the information generated by the radar without any processing. To this end, we have created the following custom ROS messages: `ObjectList`, `DetectionList` and `Status` (see Figure 2a), which are a direct translation of

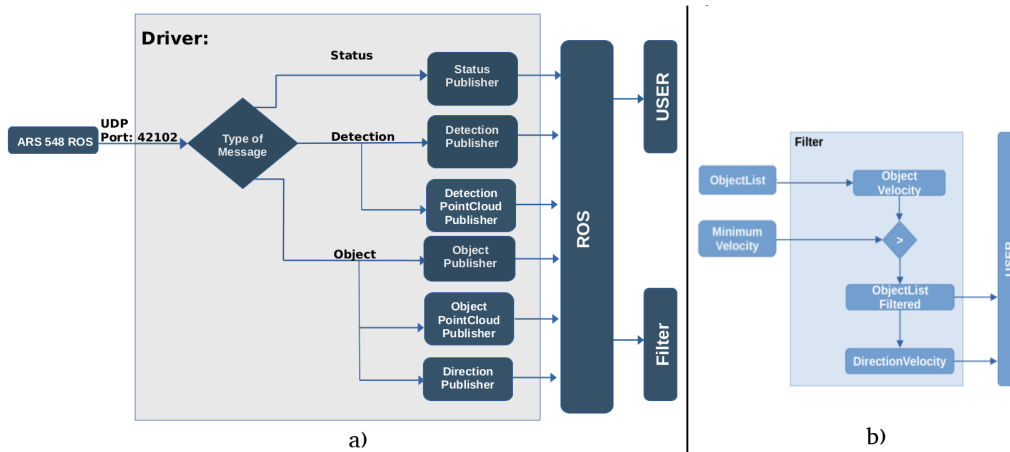


Figure 2: a) Basic flow diagram of ARS 548 driver. b) Example application of the filter: detection of objects moving faster than a threshold velocity.

the data structures send by the sensor as described in the ARS 548 reference manual [15]. The messages have been included in Appendix A for the sake of completeness. Finally, we can use the advanced information available in the Objects structure to filter them, so that only the required objects are taken into consideration (see Figure 2b and Section 2.2.3).

2.1 Software architecture

Our solution consists of two ROS packages, with the following main functionalities:

- *ARS548_driver*. This folder contains the libraries, code and functions needed for the actual driver to work. In particular, the `ars_548` driver node receives the data from the radar via Ethernet link and transforms it into standard messages and custom messages (defined in *ARS548_messages*), which are provided to the user via ROS middleware. On the other hand, `ars_548_filter` enables the user to distinguish different types of objects thanks to the advanced functionalities of the sensor.
- *ARS548_messages*. In this folder we define the custom messages that are sent by our driver. These messages follow the data structure of the messages generated by the radar, as defined in [15].

The full driver source code is publicly available in our GitHub repository [16]. Also, please refer to Appendix B for the additional contents associated with the paper.

2.2 Software functionalities

This section highlights the main functionalities provided by ARS 548 driver.

2.2.1 Reception and translation of messages.

The proposed driver is able to establish a UDP connection with the sensor and translate the different information from the sensor to custom and standard ROS messages, making the necessary endian translations by means of templated C++ functions.

With this functionality we provide the user with all the information from ARS548 as emitted by the sensors with our custom messages. Additionally, we provide standard messages which are easier to visualize and process with standard ROS packages.

2.2.2 Visualization of the results.

By generating the `PointCloud2` and `PoseArray` standard ROS messages, the user can easily represent the objects in the standard ROS visualizer (RViz [17]). To this end, we provide the user with custom visualization configurations that can be loaded in RViz for easily representing the measurements from the radar sensor (see Figure 2a). You can see an example of representation of the radar measurements in Figure 3.

2.2.3 Object filtering

The `ars548_ros` package provides the user with a filter able to interpret our custom messages and to provide filtered point clouds depending on the extended information generated by the sensor. The available information is defined in the `Object` message described in Appendix A. The filter can easily be customized via inheritance just by overriding a method; please refer to our repository for more details. As an example, see Section 3.2 in which we used a filter to represent only moving vehicles in the environment using the speed estimation from the sensor.

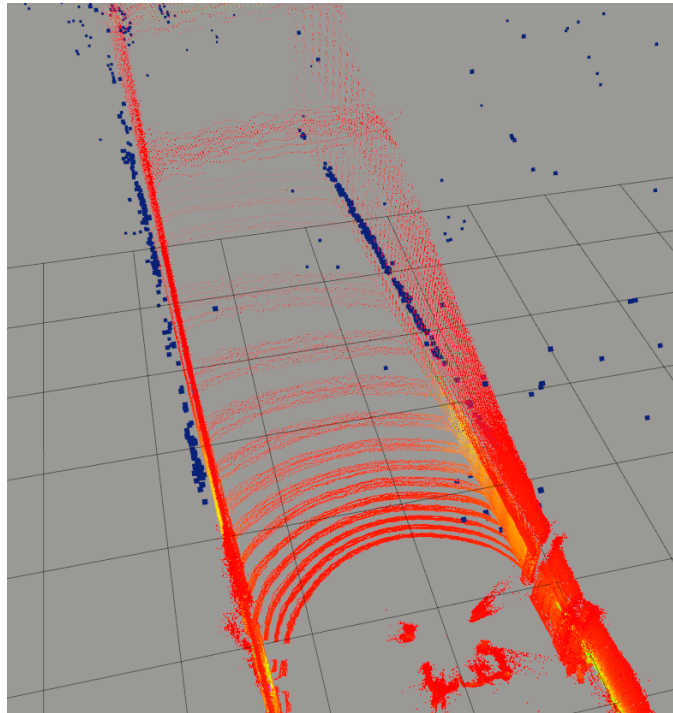


Figure 3: Radar detection measurements captured by the ARS 548 RDI sensor in blue and OS1 liDAR measurements in red. Please note the alignment between LiDAR and radar measurements.

3 Illustrative examples

The driver presented in this paper has been experimentally tested in field experiments with the robotic ARCO platform [18] (see Figure 4). In particular, we describe here two example scenarios. First, a traffic monitoring scenario, in which the velocity estimation offered by the radar sensor can be of great use to distinguish the road traffic from the background. Second, a typical robotic scenario, in which the robot should be capable of both generating a map of the environment and localizing itself on it, in a problem that is usually referred as Simultaneous Localization and Mapping (SLAM).

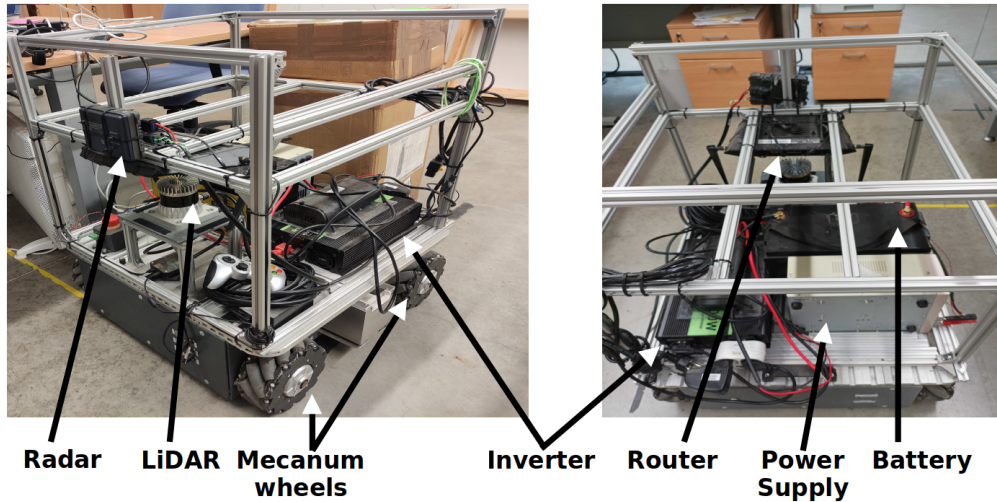


Figure 4: Our ARCO robotic platform equipped with both an ARS 548 RDI sensor and an OS1-32 LiDAR sensor. The necessary equipment for the experiments is pointed out on the Figure.

3.1 Experimental setup

Our ARCO robotic platform has been equipped with an ARS 548 RDI sensor and an OS1-32 LiDAR sensor, which was used as a reference to confirm the validity of the measurements obtained by the radar sensor (see Figure 4). We used an MSI GF62 7RE Laptop with 32GB RAM and Intel Core i7 processor connected to both sensors via Ethernet, with independent connections. For each experiment, we generated one or more ROSBag files with all the information from both sensors. In particular, with regards to ARS 548 RDI, we saved both our custom topics and the standard ones. The dataset is available at [2].

3.2 Experiment 1. Traffic monitoring

In this experiment, our ARCO robotic platform remained static in the proximity of a road. The objective here is to use the ARS 548 RDI sensor to monitor the road traffic nearby, taking advantage of its medium-long range (up to 300m) and its capability of measuring the speed of the detected objects. We use the object filtering feature of our driver (see Figure 2b) obtaining an

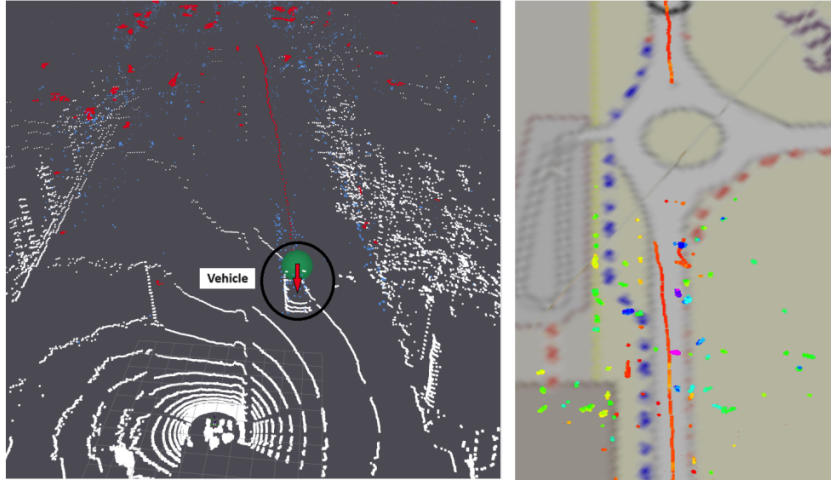


Figure 5: Snapshot of Experiment 1. (left) Radar detections on blue, Radar objects on red, Radar object moving faster than 10 km/h on a green sphere and LiDAR measurements on white. (right) Geolocalized radar measurements represented over a map from OpenStreetMap [19]. Red lines represent cumulative radar detections of two different vehicles over the map of the environment.

object point cloud that contains vehicles moving faster than 10 km/h, which are assumed as road traffic (see Figure 5).

3.3 Experiment 2. SLAM

In the second experiment, our ARCO robotic platform navigates within an open environment while estimating its trajectory through the information received by the radar. Figure 3 illustrates the alignment between the measurements from our driver and the LiDAR, verifying its proper functioning. To validate the results of this experiment, we have employed the odometry generated by the LeGO-LOAM package [20] as a baseline, which relies on the LiDAR sensor for data acquisition (see Figure 6). The data acquired from both the radar and LiDAR sensors will be used for future odometry and SLAM techniques, ensuring accurate mapping and localization, especially in hazardous scenarios where radar is employed.

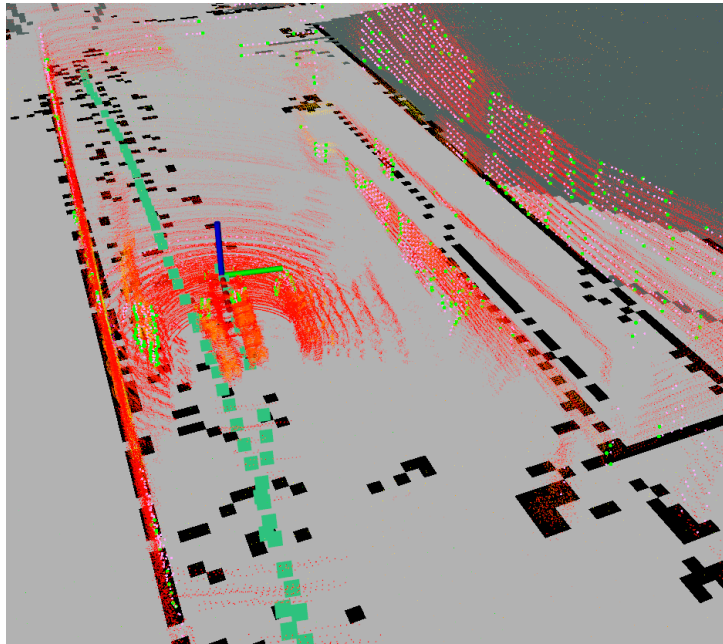


Figure 6: The baseline trajectory generated by the LeGO-LOAM package is represented in large green dots over the generated map projection in 2D. The LiDAR measurements are represented in red dots, with small green dots representing features detected by Lego-LOAM.

4 Impact

This open source driver has been published under the BSD 3-Clause License in the hope of minimizing the development efforts of all users of the ARS 548 RDI sensor who would like to implement ROS-based applications with it. By doing so, the users can easily setup the driver and acquire its data with ROS interfaces and then focus on processing the data as needed for their own experiments, significantly speeding up their research and development process.

Our main goal is to use this device for inspection robotics application carried out in reduced visibility environments, mainly due to weather phenomena such as rain, fog and snow or emergency situations involving smoke. These applications may include the inspection of different facilities such as offshore oil&gas extraction plants, sewers and transmission and electric power lines

[21]. By using this sensor, we can ensure that inspection operations can be performed safely under all circumstances.

Another application field is autonomous driving. In fact, this is the main area of application for the ARS 548 RDI devices. The idea here is to incorporate this sensor into an autonomous vehicle to provide it with detailed information of surrounding objects including the type of object or vehicle and its relative velocity and acceleration. With this information, the user can design collision detection and resolution algorithms that guarantee the collision-free operation of the vehicle in spite of harsh weather or poor illumination circumstances.

5 Conclusions

This paper described a ROS driver to configure and interface with the ARS 548 RDI radar sensor. The driver works on both ROS and ROS2 versions, maximizing its impact on the community. The driver has been tested in two different field experiments, showcasing the advanced information from the sensor and the filtering capabilities of our driver.

Future work will focus on developing new radar odometry approaches, and LiDAR-radar data fusion mechanisms.

Declaration of competing interest

The authors declare that they have no known competing financial interests or personal relationships that could have appeared to influence the work reported in this paper.

Data availability

All the data used in this paper is openly available at [2].

Acknowledgements

Authors would like to thank Fernando Amodeo for his invaluable help. This work has been supported by the grants INSERTION PID2021-127648OB-C31

and RATEC PDC2022-133643-C21. Both grants have been funded by the Spanish Ministry of Science, Innovation and Universities with grant number 10.13039/501100011033 and “European Union NextGenerationEU/PRTR”.

Appendix A. Custom ARS 548 messages

Below you can find the definition of the custom ROS messages in `ars548_messages`.

Detection.msg

```
1 float32 f_azimuthangle #Unaligned Detection Azimuth Angle
2 float32 f_azimuthanglestd #Azimuth Angle Std
3 uint8 u_invalidflags #Detection Invalid Flags
4 float32 f_elevationangle #Unaligned Detection Elevation Angle
5 float32 f_elevationanglestd #Elevation Angle Std
6 float32 f_range #Detection Radial Distance
7 float32 f_rangestd #Radial Distance Std
8 float32 f_rangerate #Detection Radial Velocity
9 float32 f_rangeratestd #Radial Velocity Std
10 int8 s_rcs #Detection RCS
11 uint16 u_measurementid #Detection ID
12 uint8 u_positivepredictivevalue #Existence Probability
13 uint8 u_classification #Detection Classification
14 uint8 u_multitargetprobabilitym #Multi-Target Probability
15 uint16 u_objectid #Associated Object ID
16 uint8 u_ambiguityflag #Probability for resolved velocity ambiguity
17 uint16 u_sortindex #tbd
```

DetectionList.msg

```
1 std_msgs/Header header
2 uint64 crc #Checksum (E2E Profile 7) (Reserved)
3 uint32 length #Len (E2E Profile 7) (Reserved)
4 uint32 sqc #SQC (E2E Profile 7) (Reserved)
5 uint32 dataid #Data ID (E2E Profile 7) (Reserved)
6 uint32 timestamp_nanoseconds #Timestamp Nanoseconds
7 uint32 timestamp_seconds #Timestamp Seconds
8 uint8 timestamp_syncstatus #Timestamp Sync Status
9 uint32 eventdataqualifier #Event Data Qualifier (unused)
10 uint8 extendedqualifier #Extended Qualifier (unused)
11 uint16 origin_invalidflags #Sensor Position Invalid flags (unused)
12 float32 origin_xpos #Sensor X Position with reference to rear axle
13 float32 origin_xstd #Sensor X Position STD (unused)
14 float32 origin_ypos #Sensor Y Position with reference to rear axle
15 float32 origin_ystd #Sensor Y Position STD (unused)
16 float32 origin_zpos #Sensor Z Position with reference to rear axle
17 float32 origin_zstd #Sensor Z Position STD (unused)
18 float32 origin_roll #Sensor Roll Angle (unused)
19 float32 origin_rollstd #Sensor Roll Angle STD (unused)
```

```

20 float32 origin_pitch #Sensor Pitch Angle with alignment correction
21 float32 origin_pitchstd #Sensor Pitch Angle STD
22 float32 origin_yaw #Sensor Yaw Angle with alignment correction
23 float32 origin_yawstd #Sensor Yaw Angle STD
24 uint8 list_invalidflags #Invalid flags (unused)
25 Detection[800] list_detections #Detection Array
26 float32 list_radveldomain_min #Ambiguity free Doppler velocity range Min
27 float32 list_radveldomain_max #Ambiguity free Doppler velocity range Max
28 uint32 list_numofdetections #Number of Detections
29 float32 aln_azimuthcorrection #Azimuth Alignment Correction
30 float32 aln_elevationcorrection #Elevation Alignment Correction
31 uint8 aln_status #Status of alignment

```

Object.msg

```

1  uint16 u_statussensor #tbd
2  uint32 u_id #Unique ID of object
3  uint16 u_age #Age of object
4  uint8 u_statusmeasurement #Object Status
5  uint8 u_statusmovement #Object Movement Status
6  uint16 u_position_invalidflags #tbd
7  uint8 u_position_reference #Reference point position
8  float32 u_position_x #X Position of reference point
9  float32 u_position_x_std #X Position Std
10 float32 u_position_y #Y Position of reference point
11 float32 u_position_y_std #Y Position Std
12 float32 u_position_z #Z Position of reference point
13 float32 u_position_z_std #Z Position Std
14 float32 u_position_covariancexy #Covariance X Y
15 float32 u_position_orientation #Object Orientation
16 float32 u_position_orientation_std #Orientation Std
17 uint8 u_existence_invalidflags #unused
18 float32 u_existence_probability #Probability of Existence
19 float32 u_existence_ppv #unused
20 uint8 u_classification_car #Car Classification Probability
21 uint8 u_classification_truck #Truck Classification Probability
22 uint8 u_classification_motorcycle #Motorcycle Classification Probability
23 uint8 u_classification_bicycle #Bicycle Classification Probability
24 uint8 u_classification_pedestrian #Pedestrian Classification Probability
25 uint8 u_classification_animal #Animal Classification Probability
26 uint8 u_classification_hazard #Hazard Classification Probability
27 uint8 u_classification_unknown #Unknown Classification Probability
28 uint8 u_classification_overdrivable #unused
29 uint8 u_classification_underdrivable #unused
30 uint8 u_dynamics_absvel_invalidflags #unused
31 float32 f_dynamics_absvel_x #X Absolute Velocity
32 float32 f_dynamics_absvel_x_std #X Absolute Velocity Std
33 float32 f_dynamics_absvel_y #Y Absolute Velocity
34 float32 f_dynamics_absvel_y_std #Y Absolute Velocity Std
35 float32 f_dynamics_absvel_covariancexy #Covariance Absolute Velocity X Y
36 uint8 u_dynamics_relvel_invalidflags #unused
37 float32 f_dynamics_relvel_x #X Relative Velocity
38 float32 f_dynamics_relvel_x_std #X Relative Velocity Std
39 float32 f_dynamics_relvel_y #Y Relative Velocity
40 float32 f_dynamics_relvel_y_std #Y Relative Velocity Std
41 float32 f_dynamics_relvel_covariancexy #Covariance Relative Velocity X Y

```

```

42 uint8 u_dynamics_absaccel_invalidflags #unused
43 float32 f_dynamics_absaccel_x #X Absolute Acceleration
44 float32 f_dynamics_absaccel_x_std #X Absolute Acceleration Std
45 float32 f_dynamics_absaccel_y #Y Absolute Acceleration
46 float32 f_dynamics_absaccel_y_std #Y Absolute Acceleration Std
47 float32 f_dynamics_absaccel_covariancexy #Covariance Absolute Acceleration X
  Y
48 uint8 u_dynamics_relaccel_invalidflags #unused
49 float32 f_dynamics_relaccel_x #X Relative Acceleration
50 float32 f_dynamics_relaccel_x_std #X Relative Acceleration Std
51 float32 f_dynamics_relaccel_y #Y Relative Acceleration
52 float32 f_dynamics_relaccel_y_std #Y Relative Acceleration Std
53 float32 f_dynamics_relaccel_covariancexy #Covariance Relative Acceleration X
  Y
54 uint8 u_dynamics_orientation_invalidflags #unused
55 float32 u_dynamics_orientation_rate_mean #Object Orientation Rate
56 float32 u_dynamics_orientation_rate_std #Orientation Rate Std
57 uint32 u_shape_length_status #(unused) Shape Length Status
58 uint8 u_shape_length_edge_invalidflags #(unused) Invalid Flags Shape Length
59 float32 u_shape_length_edge_mean #Mean Shape Length
60 float32 u_shape_length_edge_std #(unused) Shape Length Std
61 uint32 u_shape_width_status #(unused) Shape Width Status
62 uint8 u_shape_width_edge_invalidflags #(unused) Invalid Flags Shape Width
63 float32 u_shape_width_edge_mean #Mean Shape Width
64 float32 u_shape_width_edge_std #(unused) Shape Width Std

```

ObjectList.msg

```

1 std_msgs/Header header
2 uint64 crc #Checksum (E2E Profile 7) (Reserved)
3 uint32 length #Len (E2E Profile 7) (Reserved)
4 uint32 sqc #SQC (E2E Profile 7) (Reserved)
5 uint32 dataid #Data ID (E2E Profile 7) (Reserved)
6 uint32 timestamp_nanoseconds #Timestamp Nanoseconds
7 uint32 timestamp_seconds #Timestamp Seconds
8 uint8 timestamp_syncstatus #Timestamp Sync Status
9 uint32 eventdataqualifier #(unused) Event Data Qualifier
10 uint8 extendedqualifier #(unused) Extended Qualifier
11 uint8 objectlist_numofobjects #Number of Objects
12 Object[50] objectlist_objects #Object Array

```

Status.msg

```

1 uint32 timestamp_nanoseconds #Timestamp Nanoseconds
2 uint32 timestamp_seconds #Timestamp Seconds
3 uint8 timestamp_syncstatus #Timestamp Sync Status
4 uint8 swversion_major #Software version (major)
5 uint8 swversion_minor #Software version (minor)
6 uint8 swversion_patch #Software version (patch)
7 float32 longitudinal #Longitudinal sensor position (AUTOSAR)
8 float32 lateral #Lateral sensor position (AUTOSAR)
9 float32 vertical #Vertical sensor position (AUTOSAR)
10 float32 yaw #Sensor yaw angle (AUTOSAR)
11 float32 pitch #Sensor pitch angle (AUTOSAR)
12 uint8 plugorientation #Orientation of plug

```

```

13 float32 length #Vehicle length
14 float32 width #Vehicle width
15 float32 height #Vehicle height
16 float32 wheelbase #Vehicle wheelbase
17 uint16 maximundistance #Maximum detection distance
18 uint8 frequencyslot #Center frequency
19 uint8 cycletime #Cycle time
20 uint8 timeslot #Cycle offset
21 uint8 hcc #Country code
22 uint8 powersave_standstill #Power saving in standstill
23 uint32 sensoripaddress_0 #Sensor IP address
24 uint32 sensoripaddress_1 #Reserved
25 uint8 configurationcounter #Counter that counts up if new configuration has
    been received and accepted
26 uint8 status_longitudinalvelocity #Signals if current VDY is OK or timed out
27 uint8 status_longitudinalacceleration #Signals if current VDY is OK or timed
    out
28 uint8 status_lateralacceleration #Signals if current VDY is OK or timed out
29 uint8 status_yawrate #Signals if current VDY is OK or timed out
30 uint8 status_steeringangle #Signals if current VDY is OK or timed out
31 uint8 status_drivingdirection #Signals if current VDY is OK or timed out
32 uint8 status_characteristicspeed #(Unused) Signals if current VDY is OK or
    timed out.
33 uint8 status_radarstatus #Signals if Radar Status is OK
34 uint8 status_voltagestatus # Bitfield to report under- and overvoltage
    errors
35 uint8 status_temperaturestatus #Bitfield to report under- and
    overtemperature errors
36 uint8 status_blockagestatus #Current blockage state and blockage self test
    state.

```

Appendix B. Supplementary data

The video tutorial for configuring the sensor and the driver can be found at [22]. The repository of the driver can be found at [16] and the acquired dataset can be found at [2].

References

- [1] ARS 548 RDI. continental engineering services, <https://conti-engineering.com/components/ars-548-rdi/>, [Accessed 04-04-2024] (2023).
- [2] L. Coto, F. F. Calatayud, D. Alejo, J. J. Carpio, F. Caballero, L. Merino, ROS2 Datasets for localization and mapping algorithms — robotics.upo.es, <https://robotics.upo.es/datasets/ArcoDataset/main.html>, [Accessed 10-06-2024] (2024).

- [3] G. Brooker, R. Hennessey, C. Lobsey, M. Bishop, E. Widzyk-Capehart, Seeing through dust and water vapor: Millimeter wave radar sensors for mining applications, *Journal of Field Robotics* 24 (7) (2007) 527–557. arXiv:<https://onlinelibrary.wiley.com/doi/pdf/10.1002/rob.20166>, doi:<https://doi.org/10.1002/rob.20166>. URL <https://onlinelibrary.wiley.com/doi/abs/10.1002/rob.20166>
- [4] Y. Li, P. Duthon, M. Colomb, J. Ibanez-Guzman, What happens for a tof lidar in fog?, *IEEE Transactions on Intelligent Transportation Systems* 22 (11) (2021) 6670–6681. doi:[10.1109/TITS.2020.2998077](https://doi.org/10.1109/TITS.2020.2998077).
- [5] J. D. Gutiérrez, A. R. Jiménez, F. Seco, F. J. Álvarez, T. Aguilera, J. Torres-Sospedra, F. Melchor, Getsensordata: An extensible android-based application for multi-sensor data registration, *SoftwareX* 19 (2022) 101186. doi:<https://doi.org/10.1016/j.softx.2022.101186>. URL <https://www.sciencedirect.com/science/article/pii/S2352711022001121>
- [6] S. Khattak, C. Papachristos, K. Alexis, Keyframe-based thermal-inertial odometry, *Journal of Field Robotics* 37 (4) (2020) 552–579.
- [7] M. R. U. Saputra, P. P. de Gusmao, C. X. Lu, Y. Almalioglu, S. Rosa, C. Chen, J. Wahlström, W. Wang, A. Markham, N. Trigoni, Deep-tio: A deep thermal-inertial odometry with visual hallucination, *IEEE Robotics and Automation Letters* 5 (2) (2020) 1672–1679.
- [8] M. Mielle, M. Magnusson, A. J. Lilienthal, A comparative analysis of radar and lidar sensing for localization and mapping, in: *2019 European Conference on Mobile Robots (ECMR)*, Prague, Czech Republic, 2019, IEEE, 2019, pp. 1–6.
- [9] D. Barnes, M. Gadd, P. Murcutt, P. Newman, I. Posner, The oxford radar robotcar dataset: A radar extension to the oxford robotcar dataset, in: *2020 IEEE International Conference on Robotics and Automation (ICRA)*, 2020, pp. 6433–6438. doi:[10.1109/ICRA40945.2020.9196884](https://doi.org/10.1109/ICRA40945.2020.9196884).
- [10] M. Bijelic, T. Gruber, F. Mannan, F. Kraus, W. Ritter, K. Dietmayer, F. Heide, Seeing through fog without seeing fog: Deep multimodal sensor

- fusion in unseen adverse weather, in: 2020 IEEE/CVF Conference on Computer Vision and Pattern Recognition (CVPR), 2020, pp. 11679–11689. doi:10.1109/CVPR42600.2020.01170.
- [11] Z. Hong, Y. Petillot, S. Wang, Radarslam: Radar based large-scale slam in all weathers, in: 2020 IEEE/RSJ International Conference on Intelligent Robots and Systems (IROS), 2020, pp. 5164–5170. doi:10.1109/IROS45743.2020.9341287.
- [12] D. Alejo, R. Rey, J. A. Cobano, F. Caballero, L. Merino, Data Fusion of RADAR and LIDAR for Robot Localization Under Low-Visibility Conditions in Structured Environments, in: D. Tardioli, V. Matellan, G. Heredia, M. Silva, L. Marques (Eds.), ROBOT2022: Fifth Iberian Robotics Conference, Vol. 592 of Advances in Intelligent Systems and Computing, Springer International Publishing, 2023, pp. 301–313.
- [13] E. B. Quist, R. W. Beard, Radar odometry on fixed-wing small unmanned aircraft, IEEE Transactions on Aerospace and Electronic Systems 52 (1) (2016) 396–410. doi:10.1109/TAES.2015.140186.
- [14] S. Macenski, T. Foote, B. Gerkey, C. Lalancette, W. Woodall, Robot operating system 2: Design, architecture, and uses in the wild, Science Robotics 7 (66) (2022) eabm6074. arXiv:<https://www.science.org/doi/pdf/10.1126/scirobotics.abm6074>, doi:10.1126/scirobotics.abm6074.
URL <https://www.science.org/doi/abs/10.1126/scirobotics.abm6074>
- [15] RadarSensors_Annex_Interface_ARS548RDI. ARS548 Ethernet Interface (2024).
- [16] F. Fernández-Calatayud, J. J. Carpio, D. Alejo, F. Caballero, L. Merino, ROS2 driver for the Continental ARS548 Radar 4D, https://github.com/robotics-upo/ars548_ros, [Accessed 27-03-2024] (2024).
- [17] H. R. Kam, S.-H. Lee, T. Park, C.-H. Kim, Rviz: a toolkit for real domain data visualization, Telecommun. Syst. 60 (2) (2015) 337–345. doi:10.1007/s11235-015-0034-5.
URL <https://doi.org/10.1007/s11235-015-0034-5>

- [18] R. Rey, J. A. Cobano, M. Corzetto, L. Merino, P. Alvito, F. Caballero, A novel robot co-worker system for paint factories without the need of existing robotic infrastructure, *Robotics and Computer-Integrated Manufacturing* 70 (2021) 102122. doi:<https://doi.org/10.1016/j.rcim.2021.102122>. URL <https://www.sciencedirect.com/science/article/pii/S0736584521000089>
- [19] OpenStreetMap contributors, Planet dump retrieved from <https://planet.osm.org> , <https://www.openstreetmap.org> (2017).
- [20] T. Shan, B. Englot, Lego-loam: Lightweight and ground-optimized lidar odometry and mapping on variable terrain, in: *IEEE/RSJ International Conference on Intelligent Robots and Systems (IROS)*, IEEE, 2018, pp. 4758–4765.
- [21] W. Wang, Z. Shen, Z. Zhou, A novel vision- and radar-based line tracking assistance system for drone transmission line inspection, *Remote Sensing* 16 (2) (2024). doi:10.3390/rs16020355. URL <https://www.mdpi.com/2072-4292/16/2/355>
- [22] Robotics Lab. Universidad Pablo de Olavide, Driver installation tutorial for the radar ARS 548, <https://youtu.be/vByzrxY0N2k> (2024).

List of Figures

1	Continental ARS 548 RDI high resolution radar sensor.	4
2	a) Basic flow diagram of ARS 548 driver. b) Example application of the filter: detection of objects moving faster than a threshold velocity.	5
3	Radar detection measurements captured by the ARS 548 RDI sensor in blue and OS1 liDAR measurements in red. Please note the alignment between LiDAR and radar measurements. .	7
4	Our ARCO robotic platform equipped with both an ARS 548 RDI sensor and an OS1-32 LiDAR sensor. The necessary equipment for the experiments is pointed out on the Figure. .	8

5	Snapshot of Experiment 1. (left) Radar detections on blue, Radar objects on red, Radar object moving faster than 10 km/h on a green sphere and LiDAR measurements on white. (right) Geolocalized radar measurements represented over a map from OpenStreetMap [19]. Red lines represent cumulative radar detections of two different vehicles over the map of the environment.	9
6	The baseline trajectory generated by the LeGO-LOAM package is represented in large green dots over the generated map projection in 2D. The LiDAR measurements are represented in red dots, with small green dots representing features detected by Lego-LOAM.	10